Volume 1 | Number 1 | Jan 2013 | Pages 1–100

Journal of
Materials Chemistry A

Materials for energy and sustainability
www.rsc.org/materialsA

Li⁺

ROYAL SOCIETY
OF CHEMISTRY

ROYAL SOCIETY
OF CHEMISTRY

www.rsc.org/materialsA

Journal of Materials Chemistry A

Dynamic Article Links ▶

COMMUNICATION

Carbon Embedded α-MnO₂@Graphene Nanosheet Composite: A Bifunctional Catalyst for High Performance Lithium Oxygen Batteries†

Yong Cao, [a‡] **Ming-sen Zheng,** [a‡]***** **Senrong Cai,** [a] **Xiaodong Lin,** [a] **Cheng Yang,** [a] **Weiqiang Hu** [a] **and Quan-feng Dong** [a]*

Carbon is essential for the oxygen electrode in non-aqueous lithium oxygen (Li-O₂) batteries for improving the electron conductivity of the electrode. But it also brings some side-
10 **reactions when exposed to the Li₂O₂ product and the electrolyte, limiting the round-trip efficiency and coulombic efficiency of the batteries. In this paper, a carbon embedded α-MnO₂@graphene nanosheet (α-MnO₂@GN) composite was introduced as a highly effective catalyst for Li-O₂ batteries.**
15 **X-ray photoelectron spectroscopy (XPS) analysis showed that the Li₂CO₃ by-product was significantly reduced due to the isolation of the carbon with the electrolyte and Li₂O₂. It thus could deliver a reversible capacity of ~2413 mAh/g based on the total mass of the composite with extremely high discharge**
20 **voltage of ~2.92 V (only 40 mV lower than the thermodynamic potential) and low charge voltage of ~3.72 V at the current density of 50 mA/g. The round-trip efficiency is calculated to ~78% with a coulombic efficiency of almost 100%.**

Introduction

25 Efficiency utilization of the clean energy, such as the solar and wind power, is becoming more and more urgent due to the greenhouse effect resulted from the increasing consumption of unrenewable fossil fuels.[1] Owing to the intermittent nature of the solar and wind power, electrochemical energy storage devices
30 were widely used in green grid.[2, 3] Recently, the rechargeable non-aqueous Li-O₂ battery have attracted numerous attentions owing to its extremely high theoretical energy density of 5200 Wh/Kg based on the reaction $Li + O_2 \rightarrow Li_2O_2$ (E^0=2.96 V).[4-8] In
35 a typical non-aqueous Li-O₂ battery, the oxygen molecular is reduced to Li₂O₂ by combining with the lithium ions and electrons at the discharging process (oxygen reduction reaction, ORR), and recovered at the subsequent charging process (oxygen evolution reaction, OER). A catalyst is necessary for Li-O₂
40 batteries due to the sluggish kinetics of the oxygen cathode that would result in poor rate capability and low round-trip energy efficiency.[9-11] Numerous efforts have been paid to design and synthesize highly effective catalysts for both ORR and OER processes.[12-20]
45 Carbon is the most important material for the oxygen electrode due to that it can act as both the conductive matrix and catalyst

for the electrochemical reactions.[21-23] Various carbon materials, such as carbon nanotubes (CNTs), graphene et al., have been investigated as the oxygen catalyst for Li-O₂ batteries.[15, 24-26]
50 They exhibited excellent catalytic activity for ORR with an overpotential of ~0.2 V, but poor catalytic activity for OER with an overpotential larger than 1 V.[15, 27,25] In the past few years, transition metal oxides (TMOs) have also been intensively investigated as the oxygen electrode catalyst for Li-O₂ batteries
55 since Bruce and co-workers found the catalytic activity of manganese oxides.[28-33] Among them, α–MnO₂ is considered as the most promising catalyst for Li-O₂ batteries due to its low cost, environmental friendliness, and moderate activity.[29, 34] But the round-trip efficiency of the TMO catalysts is still less than 70%.
60 Furthermore, Li₂CO₃ by-product generated from the side reactions and electrolyte decomposition on the carbon surface may increase the OER overpotential and lead to the cycle deterioration.[22, 35, 36] To improve the round-trip efficiency, precious metal or metal oxides, such as Au, Pd, Ru and RuO₂,
65 have demonstrated excellent catalytic activity for OER with ultra-low charge overpotential, but they may suffer from the high cost and scarce resources in long term.[37-40] To avoid the formation of Li₂CO₃, some oxygen cathodes without carbon or with carbon defects coated demonstrated significant improvement of the
70 electrochemical performance by alleviating the side reactions. By coating the carbon defects with Al₂O₃, Amine et al. developed a Pd/Al₂O₃/Super P nanostructured cathode with a charge overpotential of only 0.2 V.[41] Carbon-free catalysts, such as porous Au, (Co, Mn)₃O₄ nanowires@Ni, Ru/ITO and Ru/STO
75 cathodes, also exhibited high round-trip efficiency and improved cycle stability.[37, 42-44]
Herein, a carbon embedded α-MnO₂@GN composite was developed and investigated as the oxygen electrode catalyst for Li-O₂ batteries. The α-MnO₂@GN composite was synthesized by
80 the reaction between KMnO₄ and graphene. Only 8% mass content of graphene was introduced in the composite and was fully covered by MnO₂ particles, which would prevent the side reaction on the surface of graphene. Resulting from the significant reduction of Li₂CO₃ formation, the α-MnO₂@GN
85 composite exhibited superior catalytic activity for both ORR and OER processes. It could deliver a reversible capacity of ~2413 mAh/g based on the total mass of the composite at the current density of 50 mA/g with a round-trip efficiency up to ~78%. The average discharge voltage was as high as 2.92 V with an

overpotential of only 40 mV, and the onset voltage of charge process was significantly reduced to 3.0 V.

Results and discussion

The structure and morphology of the α-MnO_2@GN composite
5 was characterized by X-ray diffraction method and scanning electron microscopy (SEM). **Fig. 1a** exhibits the XRD pattern of the α-MnO_2@GN composite. The peaks can be indexed well to tetragonal α-MnO_2 phase (space group I4/m, JCPDS 01-072-1982), which is consistent with our previous work.[28] The urchin-
10 like α-MnO_2@GN composite with ~500 nm in diameter is composed of uniform MnO_2 nanorods with ~100 nm in length and 10 nm in width, as shown in **Fig. 1b**, implying a large specific surface area of the composite. The MnO_2 nanorods are connected with each other and no graphene is observed in the
15 SEM images. The SEM and HRTEM images of α-MnO_2 nanorods are provided in **Fig. S1** (†ESI). The clear lattice fringes illustrate that the interlayer space is about 0.698 nm, corresponding to the [110] plane of α-MnO_2 which is the crystallographic direction of the MnO2 nanorod.[45]
20 As mentioned above, the α-MnO_2@GN composite was synthesized by the reaction between $KMnO_4$ and graphene. The thermogravimetric analysis (TGA) result shown in **Fig. S2** demonstrates a carbon content of ~8% in the composite. Energy dispersive X-ray spectroscopy (EDS) analysis was carried out to
25 confirm the elemental component and distribution of the composite. **Fig. 2** show the EDS spectra of the α-MnO_2@GN composite, revealing that the composite contains Mn, O, C elements, and the contents of Mn, C, O are 56.01%, 5.35% and 38.64%. The EDS elemental mapping confirms the homogeneous
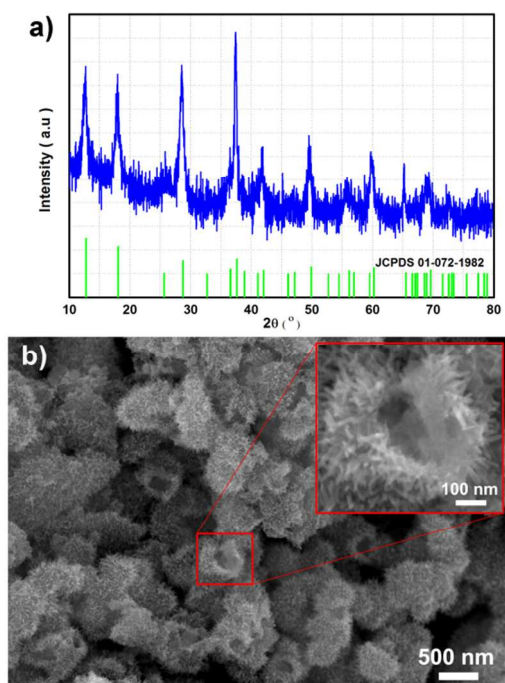30 distribution of Mn, C, O elements throughout the composite,

Fig. 1 a) X-ray diffraction pattern of the α-MnO_2@GN composite. b) An SEM image of the α-MnO_2@GN composite, inset image distinctly displays the detail structure of the urchin-like composite.
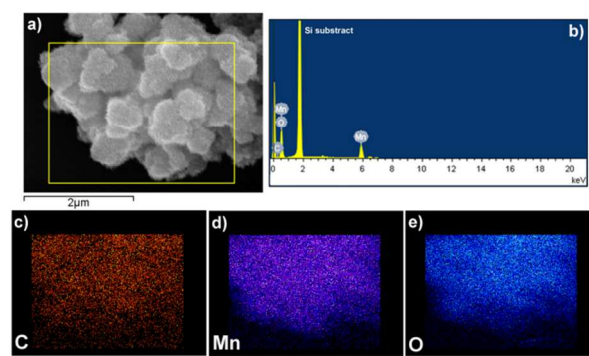

35 **Fig. 2** SEM-EDS mapping result of the α-MnO_2@GN composite and the corresponding elemental distributions of C, Mn and O.

which is also confirmed by a high-angle annular dark-field (HADDF) image and the corresponding EDS linear scanning
40 result obtained by a Tecnai F30 transmission electron microscope shown in **Fig. S3**. These suggest that the graphene is fully covered by the α-MnO_2 nanorods and embedded in the composite due to the uniformly growth of the α-MnO_2 nanorods on the surface of graphene. The pore structure of the α-
45 MnO_2@GN composite was characterized by nitrogen adsorption-desorption isotherm, as shown in **Fig. S4**. The BET surface area and pore volume are calculated to be 124.4 m^2/g and 0.732 cm^3/g, respectively, both of which are about twice as large as that of the MnO_2 nanorods. The larger surface area of the α-MnO_2@GN
50 composite would reduce the reaction resistance and the introduction of the embedded graphene would increase the electronic conductivity of the composite, which would improve the electrochemical performance. Furthermore, the pore size of the α-MnO_2@GN composite is as large as ~20 nm, which would
55 facilitate the diffusion of the oxygen and electrolyte in the electrode.

The electrochemical performance of as-prepared α-MnO_2@GN composite was evaluated by the galvanostatic discharge/charge method and compared with that of the α-MnO_2 nanorod and
60 pristine graphene cathodes. The cells were measured between 2.2 V and 4.2 V (vs. Li /Li^+) at the current density of 50 mA/$g_{cathode}$, as shown in **Fig. 3a**. The α-MnO_2@GN composite can deliver the highest capacity of 2413 mAh/g based on the total weight of the catalyst among the three as-prepared cathodes, which is ~30125
65 mAh/g based on the mass of carbon. It is slightly higher than that of the pristine graphene cathode (2142 mAh/g), but significantly larger than that of the α-MnO_2 nanorod cathode (1560 mAh/g). It should be noted that the α-MnO_2@GN composite cathode also exhibits the best catalytic activity with the lowest overpotentials
70 for both ORR and OER processes. The average ORR voltage of the α-MnO_2@GN composite cathode at the current density of 50 mA/g is about 2.92 V, which is evidently higher than 2.75 V for the pristine graphene and 2.56 V for the α-MnO_2 nanorod. Noted, it is only ~40 mV lower than the thermodynamic equilibrium
75 potential based on the reaction $2Li^+ + O_2 + 2e^- \rightarrow Li_2O_2$ (E^0=2.96 V). To the best of our knowledge, it is also the lowest ORR overpotential among the currently reported catalysts.[29, 43, 46] The α-MnO_2@GN composite also exhibits the best catalytic activity for OER process with an average charge potential of 3.72 V,
80 which is ~0.16 V and 0.33 V lower than that of the pristine graphene and the α-MnO_2 nanorod, respectively. Moreover, the
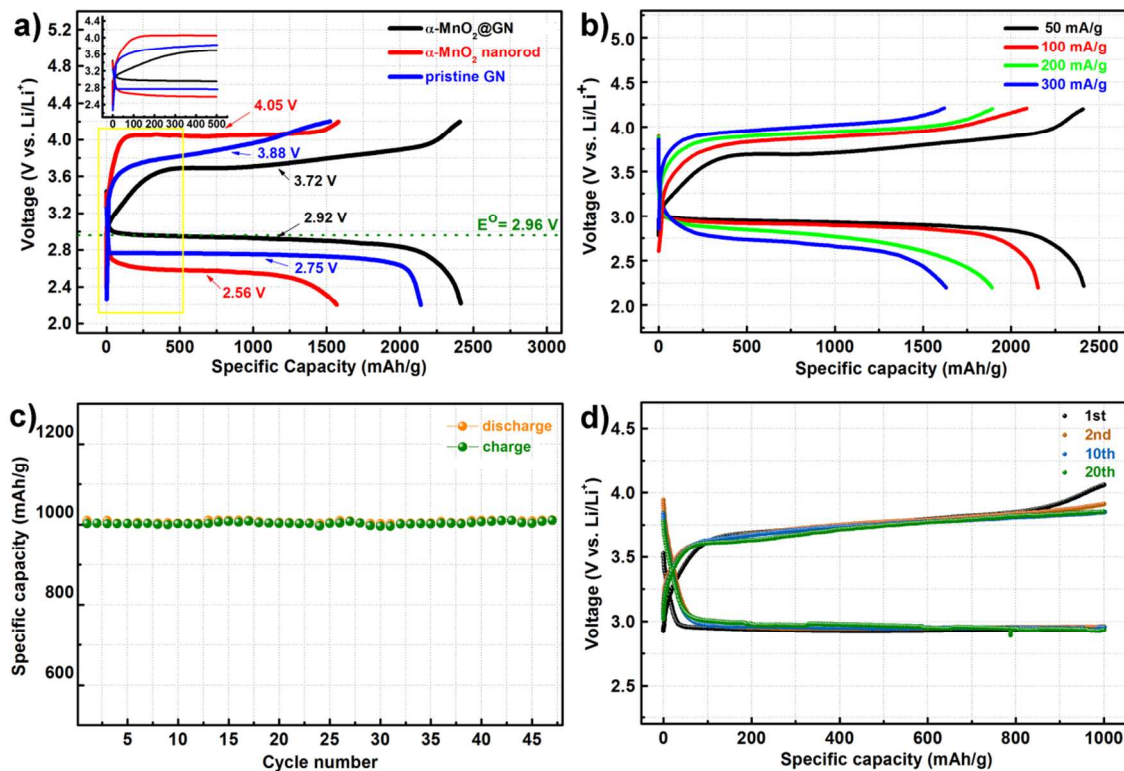
Fig. 3 a) A comparison of the discharge/charge voltage profiles of the α-MnO$_2$@GN composite, α-MnO$_2$ nanorods and the pristine graphene electrodes at the current density of 50 mA/g. Inset is the enlarged image of the selected yellow box area. b) Voltage profiles of deeply discharged/charged Li-O$_2$ batteries with the α-MnO$_2$@GN composite under different current densities from 50 mA/g to 300 mA/g (based on the total catalyst), within the voltage window of 2.2-4.2 V. c) Cyclic performance of a Li-O$_2$ battery utilizing the α-MnO$_2$@GN composite at 100 mA/g with a cut-off capacity of 1000 mAh/g. d) Voltage profile of the selected cycles in Figure 3c.

coulombic efficiency of the α-MnO$_2$@GN composite is measured to be 99.8% with the charge capacity of 2409 mAh/g at the cut-off voltage of 4.2 V, which is similar to that of the α-MnO$_2$ nanorods cathode, implying no obviously side reaction occurred on the MnO$_2$ surface. As comparison, the coulombic efficiency of the pristine graphene is only 71.1 % with the charge capacity of 1500 mAh/g. It suggests that the irreversible side reaction mainly occurs on the carbon surface and it is an effective strategy to reduce the side reaction by avoiding the direct contact of the carbon with electrolyte and Li$_2$O$_2$ through the α-MnO$_2$ covering. Benefit from the high catalytic activity and high coulombic efficiency, the round-trip efficiency of the α-MnO$_2$@GN composite is up to 78%, which is the best value among the precious-metal free catalysts.[29, 46-48] In particular, the onset potential of the α-MnO$_2$@GN composite during the OER process is ~3.0 V shown in the inset image of **Fig. 3a**, which is significantly lower than ~3.4 V of the α-MnO$_2$ nanorod and the pristine graphene, and only ~40 mV higher than the thermodynamic equilibrium potential, indicating the superior OER catalytic activity.

To further investigate the rate performance of the α-MnO$_2$ @GN composite, it was tested at various current densities from 50 mA/g to 300 mA/g. As shown in **Fig. 3b**, the α-MnO$_2$@GN composite exhibits excellent rate capability with the discharge capacities of 2153 mAh/g, 1886 mAh/g and 1632 mAh/g at the current density of 100 mA/g, 200 mA/g and 300 mA/g,

respectively, corresponding to the capacity retentions of 89.3%, 78.3% and 67.7%. The average discharge/charge voltages of the cathode are 2.92/3.72 V, 2.89 /3.88 V, 2.79/3.93 V and 2.7/3.98 V at the current densities of 50 mA/g, 100 mA/g, 200 mA/g and 300 mA/g, respectively. All the coulombic efficiency at the various current densities is ~100%, indicating the excellent stability of the α-MnO$_2$@GN composite. It should be noted that the charge/discharge time at the current density of 300 mA/g is only ~5 hours, which is possible to meet the needs for the practical application in electric vehicles. The cycle performance of the α-MnO$_2$@GN composite was evaluated at the current density of 100 mA/g with a cut-off capacity of 1000 mAh/g, which was about half of the discharge depth. As depicted in **Fig. 3c**, the α-MnO$_2$@GN composite exhibits superior cycle stability with no capacity decay being observed over 47 cycles, as well as with the coulombic efficiencies of ~100%. The selected discharging-charging voltage profiles of the 1st, 2nd, 10th, 20th cycles are shown in **Fig. 3d**. No increasing polarization could be observed on the voltage profiles during the cycles, confirming the superior cycle stability of the α-MnO$_2$@GN composite. The average discharging/charging voltages are ~2.95 V and ~3.75 V, respectively. The overpotentials of both the ORR and OER processes are even slightly lower than that of the full discharging/charging curves at the same current density due to the controlled discharge depth.

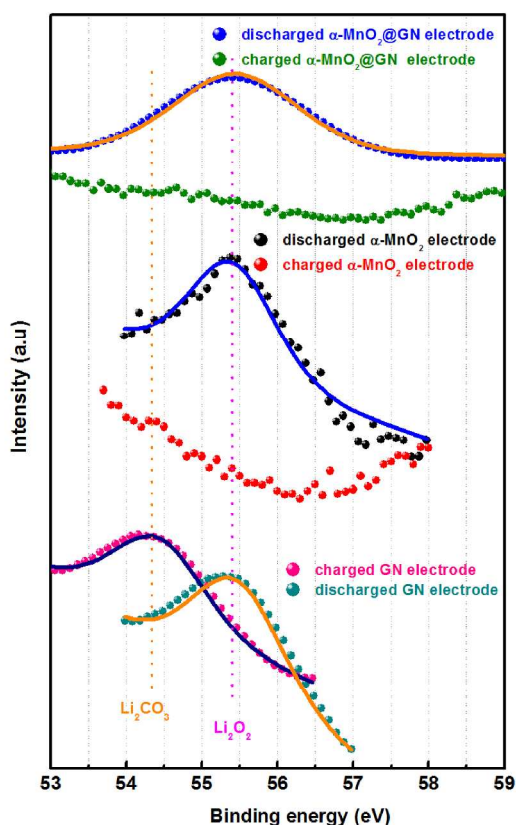To identify the component of the product on the surface of the as-

Fig. 4 Li1s spectra of the discharged/charged α-MnO₂@GN composite, α-MnO₂ nanorod and pristine graphene electrodes.

prepared cathodes during the discharging/charging processes, X-ray photoelectron spectroscopy (XPS) analysis was explored. The α-MnO₂@GN composite, the α-MnO₂ nanorod, and the pristine graphene cathodes were discharged/charged between 2.2 V and 4.2 V at the current density of 50 mA/g. **Fig. 4** shows the Li 1s XPS spectra of the cathodes at 2.2 V (discharged state) and 4.2 V (charged state). Only one peak at about 55.4 eV assigned to Li-O bond of Li_2O_2 was observed in the spectra of all three cathodes after being discharged to 2.2 V.[46] It suggests that Li_2O_2 is the main discharge product on either the surface of MnO_2 or carbon, and no obvious side reaction occurred during the discharging process in the DMSO based electrolyte. The Li 1s peak in the spectrum of the α-MnO₂@GN composite disappeared when the cathode was charged back to 4.2 V, as well as in that of the α-MnO₂ nanorod cathode, implying the full decomposition of Li_2O_2 on the surface of both the α-MnO₂@GN composite and the α-MnO₂ nanorod. Meanwhile, no other peaks appeared in the spectra of the α-MnO₂@GN composite and the α-MnO₂ nanorod cathodes, implying no evident side reaction occurred. As a comparison, a new peak at about 54.5 eV appeared in the spectrum of the charged pristine graphene cathode, which can be assigned to the Li-O bond in Li_2CO_3, although the Li_2O_2 peak also disappeared.[46] It demonstrates that Li_2O_2 is electrochemically reversible, and the Li_2CO_3 side product is formed mainly at the charging (or OER) process due to the reaction between Li_2O_2 and carbon, resulting in the irreversible capacity loss of the cathode and low round-trip efficiency.[22] It is

consistent with the results of the galvanostatic discharge/charge results. All the above results indicate that (1) the side reactions of the oxygen cathode take place mainly at the OER process on the surface of carbon; (2) the side reaction could be significantly reduced by preventing the direct contact of carbon from the electrolyte and Li_2O_2; (3) the graphene supported MnO_2 cathode with carbon embedded exhibited improved and superior electrochemical performance as the side reaction depressed. The Mn 2p XPS spectra of α-MnO₂@GN composite were also collected and displayed in **Fig. S5**. The location of Mn2p peaks (641.8 eV for Mn 2p3/2 and 653.6 eV for Mn 2p1/2), as showing in the discharged state, show almost no shift in comparison with that of the charged state, although its intensity is significantly reduced due to the deposition of Li_2O_2 on the surface. Noted, the intensity of Mn 2p peaks recovered when the cathode was charged back to 4.2 V, indicating the full decomposition of Li_2O_2 and the stability of the MnO_2 during the ORR/OER processes.

Conclusions

In summary, a carbon embedded α-MnO₂@GN composite was developed as the oxygen electrode catalyst for non-aqueous Li-O₂ batteries. XPS analysis showed that no obvious side reactions took place on the surface of the α-MnO₂@GN composite due to the graphene being fully embedded in the composite. Owing to the side reaction depressing and the high conductivity of graphene supporting, the α-MnO₂@GN composite exhibited superior catalytic activity for both ORR and OER processes. It could deliver a capacity of 2413 mAh/g with a high round-trip efficiency up to ~78%, which is only reported by using the precious metal based catalysts. The average ORR potential of the composite at 50 mA/g$_{composite}$ is measured to be ~2.92 V at the current density of 50 mA/g, which is the best value to date, and the onset OER potential is as low as 3.0 V. The α-MnO₂@GN composite also exhibited excellent rate capability with the capacity of 1632 mAh/g at the current density up to 300 mA/g, and the excellent cycle stability with almost 100% capacity retention after 47 cycles. The superb performance of the α-MnO₂@GN composite along with its low cost and environmental friendliness would promote the practice application of Li-O₂ batteries.

Notes and references

[a] Department of Chemistry, College of Chemistry and Chemical Engineering, Xiamen University, State Key Laboratory of Physical Chemistry of Solid Surfaces, Xiamen University, Xiamen, Fujian, 361005, China.
† Electronic Supplementary Information (ESI) available: Experimental section; SEM and TEM images of the α-MnO₂ nanorods; HAADF image of the α-MnO₂@GN composite and the corresponding EDS linear scanning result; TG curve of the α-MnO₂@GN composite; N₂ adsorption-desorption isotherm of the α-MnO₂@GN composite and α-MnO₂ nanorods; the BJH the pore size distribution of the α-MnO₂@GN

composite; Mn2p XPS spectrums of the pristine discharged and charged α-MnO₂@GN composite electrodes. See DOI: 10.1039/b000000x/

‡ These authors contributed equally to this work.

References

1. M. I. Hoffert, K. Caldeira, G. Benford, D. R. Criswell, C. Green, H. Herzog, A. K. Jain, H. S. Kheshgi, K. S. Lackner, J. S. Lewis, H. D. Lightfoot, W. Manheimer, J. C. Mankins, M. E. Mauel, L. J. Perkins, M. E. Schlesinger, T. Volk and T. M. L. Wigley, *Science*, 2002, **298**, 981-987.
2. M. Armand and J. M. Tarascon, *Nature*, 2008, **451**, 652-657.
3. J. M. Tarascon and M. Armand, *Nature*, 2001, **414**, 359-367.
4. K. M. Abraham and Z. Jiang, *J. Electrochem. Soc.* 1996, **143**, 1-5.
5. P. G. Bruce, S. A. Freunberger, L. J. Hardwick and J.-M. Tarascon, *Nat. Mater.* 2012, **11**, 19-29.
6. E. Littauer and K. Tsai, *J. Electrochem. Soc.* 1976, **123**, 964.
7. G. Girishkumar, B. McCloskey, A. Luntz, S. Swanson and W. Wilcke, *J. Phys. Chem. Lett.* 2010, **1**, 2193-2203.
8. Y.-C. Lu, B. M. Gallant, D. G. Kwabi, J. R. Harding, R. R. Mitchell, M. S. Whittingham and Y. Shao-Horn, *Energ. Environ. Sci.* 2013, **6**, 750-768.
9. Z.-L. Wang, D. Xu, J.-J. Xu and X.-B. Zhang, *Chemical Society Reviews*, 2014, DOI: 10.1039/C3CS60248F.
10. J. Lu, L. Li, J.-B. Park, Y.-K. Sun, F. Wu and K. Amine, *Chemical Reviews*, 2014, **114**, 5611-5640.
11. B. D. McCloskey, R. Scheffler, A. Speidel, D. S. Bethune, R. M. Shelby and A. C. Luntz, *J. Am. Chem. Soc.* 2011, **133**, 18038-18041.
12. Y. Shao, S. Park, J. Xiao, J. G. Zhang, Y. Wang and J. Liu, *ACS Catalysis*, 2012, **2**, 844-857.
13. J.-L. Shui, N. K. Karan, M. Balasubramanian, S.-Y. Li and D.-J. Liu, *J. Am. Chem. Soc.* 2012, **134**, 16654-16661.
14. Y. Liang, H. Wang, J. Zhou, Y. Li, J. Wang, T. Regier and H. Dai, *J. Am. Chem. Soc.* 2012, **134**, 3517-3523.
15. B. Sun, B. Wang, D. Su, L. Xiao, H. Ahn and G. Wang, *Carbon*, 2012, **50**, 727-733.
16. Y. Cao, S.-R. Cai, S.-C. Fan, W.-Q. Hu, M.-S. Zheng and Q.-F. Dong, *Faraday Discussions*, 2014, 10.1039/C4FD00075G.
17. R. Choi, J. Jung, G. Kim, K. Song, Y.-I. Kim, S. C. Jung, Y.-K. Han, H. Song and Y.-M. Kang, *Energ. Environ. Sci.* 2014, **7**, 1362-1368.
18. Y. Cui, Z. Wen and Y. Liu, *Energ. Environ. Sci.* 2011, **4**, 4727-4734.
19. J.-H. Lee, R. Black, G. Popov, E. Pomerantseva, F. Nan, G. A. Botton and L. F. Nazar, *Energ. Environ. Sci.* 2012, **5**, 9558-9565.
20. K. Guo, Y. Li, J. Yang, Z. Zou, X. Xue, X. Li and H. Yang, *J. Mater. Chem. A*, 2014, **2**, 1509-1514.
21. R. L. McCreery, *Chemical Reviews*, 2008, **108**, 2646-2687.
22. M. M. Ottakam Thotiyl, S. A. Freunberger, Z. Peng and P. G. Bruce, *J. Am. Chem. Soc.* 2012, **135**, 494-500.
23. C. Xu, B. Xu, Y. Gu, Z. Xiong, J. Sun and X. S. Zhao, *Energ. Environ. Sci.* 2013, **6**, 1388-1414.
24. Y. Chen, F. Li, D.-M. Tang, Z. Jian, C. Liu, D. Golberg, A. Yamada and H. Zhou, *J. Mater. Chem. A*, 2013, **1**, 13076-13081.
25. J. Xiao, D. Mei, X. Li, W. Xu, D. Wang, G. L. Graff, W. D. Bennett, Z. Nie, L. V. Saraf, I. A. Aksay, J. Liu and J.-G. Zhang, *Nano Letters*, 2011, **11**, 5071-5078.
26. E. Yoo, J. Nakamura and H. Zhou, *Energ. Environ. Sci.* 2012, **5**, 6928-6932.
27. Y. Li, J. Wang, X. Li, D. Geng, R. Li and X. Sun, *Chem. Commun.* 2011, **47**, 9438-9440.
28. Y. Cao, Z. Wei, J. He, J. Zang, Q. Zhang, M. Zheng and Q. Dong, *Energ. Environ. Sci.* 2012, **5**, 9765-9768.
29. Y. Qin, J. Lu, P. Du, Z. Chen, Y. Ren, T. Wu, J. T. Miller, J. Wen, D. J. Miller, Z. Zhang and K. Amine, *Energ. Environ. Sci.* 2013, **6**, 519-531.
30. H. Wang, Y. Yang, Y. Liang, G. Zheng, Y. Li, Y. Cui and H. Dai, *Energ. Environ. Sci.* 2012, **5**, 7931-7935.
31. T. Ogasawara, A. Debart, M. Holzapfel, P. Novak and P. Bruce, *J. Am. Chem. Soc.* 2006, **128**, 1390¨C1393.
32. A. Debart, A. J. Paterson, J. Bao and P. G. Bruce, *Angew. Chem .Inter. Ed.* 2008, **47**, 4521-4524.
33. C. Sun, F. Li, C. Ma, Y. Wang, Y. Ren, W. Yang, Z. Ma, J. Li, Y. Chen, Y. Kim and L. Chen, *J. Mater. Chem. A*, 2014, **2**, 7188-7196.
34. Y. Cao, Z. Wei, J. He, J. Zang, Q. Zhang, M. Zheng and Q. Dong, *Energ Environ Sci*, 2012, **5**, 9765-9768.
35. S. A. Freunberger, Y. Chen, Z. Peng, J. M. Griffin, L. J. Hardwick, F. Bardé, P. Novák and P. G. Bruce, *J. Am. Chem. Soc.* 2011, **133**, 8040-8047.
36. B. D. McCloskey, A. Speidel, R. Scheffler, D. C. Miller, V. Viswanathan, J. S. Hummelshøj, J. K. Nørskov and A. C. Luntz, *J. Phys. Chem. Letters*, 2012, **3**, 997-1001.
37. Z. Peng, S. A. Freunberger, Y. Chen and P. G. Bruce, *Science*, 2012, **337**, 563-566.
38. H.-G. Jung, Y. S. Jeong, J.-B. Park, Y.-K. Sun, B. Scrosati and Y. J. Lee, *ACS Nano*, 2013, **7**, 3532-3539.
39. B. Sun, P. Munroe and G. Wang, *Scientific reports*, 2013, **3**. 10.1038/srep02247
40. Z. Jian, P. Liu, F. Li, P. He, X. Guo, M. Chen and H. Zhou, *Angew. Chem. Intern. Ed.* 2014, **53**, 442-446.
41. J. Lu, Y. Lei, K. C. Lau, X. Luo, P. Du, J. Wen, R. S. Assary, U. Das, D. J. Miller, J. W. Elam, H. M. Albishri, D. A. El-Hady, Y.-K. Sun, L. A. Curtiss and K. Amine, *Nat. Commun*, 2013, **4**, 10.1038/ncomms3383
42. X. Lin, Y. Shang, T. Huang and A. Yu, *Nanoscale*, 2014, **6**, 9043-9049.
43. F. Li, D.-M. Tang, Z. Jian, D. Liu, D. Golberg, A. Yamada and H. Zhou, *Adv. Mater.* 2014, **26**, 4659-4664.
44. F. Li, D.-M. Tang, Y. Chen, D. Golberg, H. Kitaura, T. Zhang, A. Yamada and H. Zhou, *Nano Letters*, 2013, **13**, 4702-4707.
45. M. Xu, L. Kong, W. Zhou and H. Li, *J. Phys. Chem. C*, 2007, **111**, 19141-19147.
46. S. Liu, Y. Zhu, J. Xie, Y. Huo, H. Y. Yang, T. Zhu, G. Cao, X. Zhao and S. Zhang, *Adv. Energy Mater.* 2014, 10.1002/aenm.201301960.
47. Z. Zhang, L. Su, M. Yang, M. Hu, J. Bao, J. Wei and Z. Zhou, *Chem. Commun.* 2014, **50**, 776-778.
48. W.-H. Ryu, T.-H. Yoon, S. H. Song, S. Jeon, Y.-J. Park and I.-D. Kim, *Nano Letters*, 2013, **13**, 4190-4197.